International Journal of Heat and Mass Transfer 77 (2014) 1063–1074

Contents lists available at ScienceDirect

International Journal of Heat and Mass Transfer

journal homepage: www.elsevier.com/locate/ijhmt

An experimental and numerical study of finned metal foam heat sinks under impinging air jet cooling

S.S. Feng [a], J.J. Kuang [a,b], T. Wen [a], T.J. Lu [a,*], K. Ichimiya [c]

[a] MOE Key Laboratory of Strength and Vibration, School of Aerospace, Xi'an Jiaotong University, Xi'an 710049, PR China
[b] School of Energy and Power Engineering, Xi'an Jiaotong University, Xi'an 710049, PR China
[c] Department of Mechanical Engineering, University of Yamanashi, 4-3-11 Kofu, Yamanashi 400-8511, Japan

ARTICLE INFO

Article history:
Received 14 September 2013
Received in revised form 20 May 2014
Accepted 27 May 2014

Keywords:
Metal foam
Finned metal foam
Heat sink
Impinging jet

ABSTRACT

This paper presents a combined experimental and numerical study on finned metal foam (FMF) and metal foam (MF) heat sinks under impinging air jet cooling. Experiments were conducted on aluminum foams of 96.3% porosity and 8 PPI (pores per inch) with four 2 mm-thickness plate fins. Different foam heights were tested at varying Reynolds numbers. Experimental results show that under a given flow rate condition, as the foam height increases, the heat transfer of MF heat sinks decreases monotonously whilst that of FMF heat sinks first increases and then slightly decreases. Under a given pumping power condition, the heat transfer of MF heat sinks is insensitive to the foam height whilst that of FMF heat sinks increases as the foam height increases. Under either a given flow rate or a given pumping power condition, the heat transfer of FMF heat sinks can be 1.5–2.8 times that of the MF heat sinks having the same height. A numerical model was also developed to simulate the conjugated heat transfer between plate-fins and metal foams in FMF heat sinks. The influence of the bonding material between metal foams and plate-fins as well as the inlet thermal boundary condition were discussed in detail using the numerical model. Comparisons of experimental and numerical results reveal that using the laminar Darcy's extended model can predict fairly both the heat transfer and pressure drop of MF and FMF heat sinks under high Reynolds numbers if the foam properties are given correctly.

1. Introduction

Jet impingement is a common method to provide high local heat transfer in a variety of applications, from electronic cooling to gas turbine cooling. The heat transfer rate to an impinging jet from a surface is a complex function of many parameters, including: jet diameter [1], jet-to-plate spacing [2], inclination angle [3], and swirling flow [4], etc. Comprehensive reviews on impinging jet heat transfer can be found in Refs. [5,6].

Another popular cooling technique is heat transfer augmentation using porous media. Open-cell metal foams, with many attractive thermal–mechanical attributes including lightweight with high strength and rigidity, high conductivity matrix, high surface area density, high permeability, and low manufacturing cost, have drawn much attentions for decades [7]. Kuo and Tien [8] presented one of the pioneer works utilizing open-cell foams to enhance liquid forced convection for electronic cooling. Hunt and Tien [9] revealed the effects of thermal dispersion as a non-Darcian phenomenon, which describes the effect of intra-pore mixing of fluid on forced convection in metal foams. Calmidi and Mahajan [10] conducted experiments and non-Darcian analysis of forced air convection in a foam filled duct. By fitting model predictions with experiments, they determined the coefficients for interstitial heat transfer coefficient and thermal dispersion conductivity. With the foam morphology idealized as inter-connected cylinders, Lu et al. [11] obtained closed-form solutions for the overall heat transfer coefficient of forced convection in metal foams bounded by two isothermal plates.

Recently, heat transfer of open-cell metal foams under impinging jet has received much attention due to the considerable heat transfer potential of combining two different cooling technologies: impinging jet and porous medium. Jeng and Tzeng [12] numerically investigated impinging cooling of metal foams under a confined slot jet. Later, the same authors extended the study by considering foam tip bypass flow, both numerically [13] and experimentally [14]. Ejlali et al. [15] numerically studied air jet impinging cooling of aluminum foams and applied the energy flux vectors for convection visualization. Marafie et al. [16] numerically investigated the non-Darcian effects on the mixed convection heat transfer in a metal-foam block with a confined slot jet. Their results illustrated

* Corresponding author. Tel.: +86 029 82665937.
E-mail address: tjlu@mail.xjtu.edu.cn (T.J. Lu).

http://dx.doi.org/10.1016/j.ijheatmasstransfer.2014.05.053
0017-9310/

Nomenclature

A_b	base area ($=LW$) (m^2)
A_{sf}	wetted surface area per volume (m^2/m^3)
c_E	form drag coefficient
c_p	specific heat (J/kg K)
d_f	fiber diameter of metal foam (m)
D	circular jet tube diameter (m)
H	height of heat sink (m)
h	overall heat transfer coefficient of heat sink (W/m^2 K)
h_{sf}	interstitial heat transfer coefficient (W/m^2 K)
h_v	volumetric heat transfer coefficient ($=h_{sf}A_{sf}$) (W/m^3 K)
I	input current of the heating pad (A)
K	permeability (m^2)
k	thermal conductivity (W/m K)
L	length of heat sink (m)
ΔP	pressure drop (Pa)
Pr	Prandtl number
Q	total heat transfer rate (W)
Re	Reynolds number
r	radial coordinate ($=(x^2+y^2)^{1/2}$) (m)
T_{in}	inlet temperature (K)
T_w	substrate temperature (K)
t	fin thickness (m)
t_b	substrate thickness (m)
U	input voltage of the heating pad (V)
u_0	inlet air velocity in the duct flow experiment (m/s)
V_j	average jet velocity (m/s)
V_{in}	inlet channel velocity ($=V_j/\sigma$) (m/s)
W	width of heat sink (m)
w	fin spacing (m/s)

Greek symbols

ρ	density (kg/m^3)
μ	viscosity (kg/ms)
ε	porosity
σ	area contraction ratio ($=w/(w+t)$)
θ	dimensionless temperature ($=(T-T_{in})/(T_w-T_{in})$)

Subscripts

f	fluid-phase
s	solid-phase
p	plate-fins

Abbreviations

MF	metal foam
FMF	finned metal foam

that the average Nusselt number increases with decreasing dimensionless height of the foam block up to 0.05, below which the Nusselt number decreases. Shih et al. [17] experimentally studied heat transfer of foam cylinders under a circular nozzle directly positioned on the foam block. They also reported that the Nusselt number first increases and then decreases as the foam height decreases. They explained that the increase of the Nusselt number is caused by the increased percentage of cooling air reaching the heated surface, due to reduced flow resistance, and the decrease of the Nusselt number is mainly caused by the reduction of the heat transfer area between the cooling air and the foam. Further, Kim et al. [18] experimentally examined heat transfer of aluminum foams under multi-air jet impingement, and Kuang et al. [19] experimentally investigated the effects of foam height and jet-to-foam distance on heat transfer of metal foams under an axial fan flow.

According to the abovementioned literature survey, a number of experimental and numerical studies have been devoted to the issue of a foam material under impinging jet cooling. However, there is no experimental validation of the numerical model by performing a combined experimental and numerical study. As the nature of turbulence in porous media is still a controversial issue [20], existing studies all used the laminar Darcy's extended model to describe impinging flow in metal foams with a small jet Reynolds number (usually Re < 1000) [13,15,16], with one exception that the jet Reynolds number was up to 40,000 [12]. For clean impinging jet flow (without porous media), when the jet Reynolds number is larger than 1000, the flow condition should be turbulent. Numerically simulating such a turbulent impinging jet is quite challenging since the following flow patterns are present in impinging jets [21]: (1) entrainment of fluid from environment; (2) relaminarization near the stagnation point; (3) large acceleration of the flow, followed by deceleration; (4) laminar–turbulent transition in the wall jet; and (5) different curve characteristics of radial heat transfer evolution, depending on flow velocities and nozzle-to-plate distances. Therefore, from an engineering point of view, is the laminar Darcy's extended model acceptable for impinging jet in foams within high Reynolds number region? To address this interesting question, a combined experimental and numerical study is carried out in this study.

By sandwiching metal foam blocks between the fins within plate-fin heat sinks, Bhattacharya and Mahajan [22,23] proposed a new type of heat sink, named as "finned metal foam (FMF)". They found that FMFs outperform metal foams by a factor between 1.5 and 2 in both forced convection and buoyancy-induced convection. Recently, using 3-D printing and investment casting techniques, Krishnan et al. [24] fabricated and studied FMF heat sinks with regular foam structures, and concluded that on an equal pumping power basis, FMF heat sinks outperform conventional plate-fin heat sinks. Above studies demonstrate the importance of FMFs for heat transfer enhancement. However, the impinging cooling characteristics of the FMFs have not been reported yet.

This paper carried out a combined experimental and numerical study on FMF and metal foam (MF) heat sinks under circular impinging air jet cooling. As the foam height has been found very important for metal foams under impinging jet cooling [17], the particular focus of this study was the influence of heat sink height on heat transfer and pressure drop of FMF heat sinks. Thermal performance of FMF heat sinks was compared with MF heat sinks under both a given flow rate and a given pumping power conditions. A numerical model was developed for FMF heat sinks, with the laminar Darcy's extended model adopted for fluid flow in porous foam with jet Reynolds number ranging from 3000 to 12,000. The model predictions were compared with test data in terms of heat transfer and pressure drop. Based on numerical results, different physical flow phenomena in metal foams and finned metal foams were revealed, and local temperature distributions were discussed in detail to explain the overall heat transfer behavior. Finally, the influence of the bonding material between metal foams and plate-fins was discussed in detail.

2. Experimental details

2.1. Fabrication of heat sinks

A FMF heat sink consists of a conventional plate-fin heat sink with aluminum foam blocks inserted into the fin gaps, as shown in Fig. 1(a). During the fabrication process, special attention was

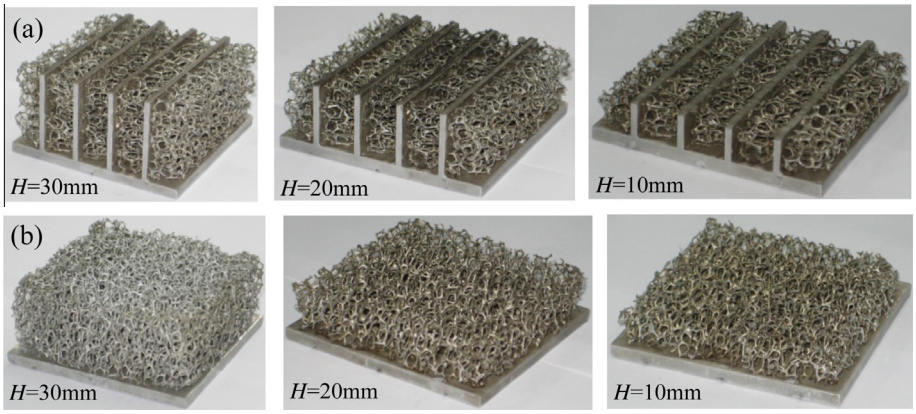

Fig. 1. Test samples: (a) finned metal foam (FMF) heat sinks; (b) metal foam (MF) heat sinks.

paid to reduce the contact thermal resistance. The fabrication process of the FMF heat sink is straightforward:

(i) cut out the plate-fin heat sink from an aluminum block using a precision wire cutting machine;
(ii) cut the foam block in size using the precision wire cutting machine to ensure a perfect fit between the fin gap and the foam block;
(iii) cover a thin layer of high conductivity thermal adhesive (Arctic Silver™, $k > 8.8$ W/m K) on the surfaces of both the fins and the substrate and then push the foam blocks into the fin gaps.

An enlarged view of the adhesive-bonded fin/foam interface is presented in Fig. 2, showing good contact between them. For comparison, regular MF heat sinks were also fabricated, as shown in Fig. 1(b).

The overall length and width of both the FMF and MF heat sinks are 68 (length) × 68 (width) mm. The thickness of the substrate is 4 mm. As shown in Fig. 1, the FMF heat sinks have four plate-fins, with fin thickness 2 mm and fin spacing 12 mm. To investigate the height effect, for FMF heat sinks, the heights studied are 40/30/20/10 mm; and for MF heat sinks, the heights studied are 30/25/20/15/10 mm. Relevant parameters of both heat sink types are listed in Table 1. The metal foam has following nominal properties: a pore size of 8 PPI (pores per inch) and a porosity of 0.963. The base material of the foam and the plate-fin heat sink is aluminum alloy, with a thermal conductivity of 202 and 170 W/m K, respectively.

2.2. Experimental setup

A test rig, as schematically shown in Fig. 3(a), was designed and built to measure the heat transfer and pressure drop characteristics

Fig. 2. Enlarged view showing adhesive-bonded interface between metal foam and plate-fin.

Table 1
Geometrical parameters of finned metal foam (FMF) and metal foam (MF) heat sinks.

	Heat sink	
	Finned metal foam	Metal foam
Length and width, $L \times W$ (mm)	68 × 68	68 × 68
Height, H (mm)	10, 20, 30, 40	10, 15, 20, 25, 30
Substrate thickness, t_b (mm)	4	4
Fin thickness, t (mm)	2	–
Fin spacing, w (mm)	12	–

of both FMF and MF heat sinks under impinging air jet. The cooling air was supplied by a blower. An air-to-air heat exchanger was used after the blower to ensure the jet exit temperature is approximately the same as the ambient temperature. The jet flow rate was measured by an orifice plate and adjustable by an inverter connected to the motor of the blower. A settling chamber was used to ensure that the jet flow is steady and uniform. The settling chamber has a dimension of 180 mm × 280 mm × 380 mm (height). A circular impinging tube, with an inner diameter of 65.7 mm (similar to the length and width of the heat sink, i.e., 68 mm), was connected to the settling chamber. There is no gap between the impinging tube and the tip of the heat sink. To prevent the bypass of air from the tip, a confinement plate was placed at the jet exit and the two side surfaces of the heat sink were shrouded with perspex plates, as shown in Fig. 3(b).

A film heating pad was attached to the bottom surface of the substrate. The heating power was controlled by setting the input voltage through a DC power supply (Agilent). The heat sink with the heating pad was then placed onto a pedestal made by Perspex ($k = 0.2$ W/m K). The pedestal consists of four layers of air gaps (gap thickness = 1 mm) separated by 5 mm thick Perspex plates. The multi-layer air gaps prevented heat loss from the pedestal. To further improve the thermal insulation, the pedestal was wrapped up with insulation foams ($k = 0.036$ W/m K). During experiments, the maximum temperature rise in the substrate was controlled lower than 15 °C. At this moderate temperature rise, the heat loss from the pedestal is negligible.

The substrate temperature, the jet exit temperature, and the ambient temperate were measured with T-type thermocouples (Omega, wire diameter: 0.127 mm). Six slots (width and depth: 1 × 1 mm) were cut from the lower surface of the substrate to house thermocouples for measuring the average temperature. To measure the heat sink inlet static pressure, four pressure tappings were mounted on the impinging tube wall near the jet exit. All the thermocouples were connected to a data acquisition system (Agilent, 34,970), and all the pressure signals were recorded by a pressure transducer (Scanivalve, DSA3217).

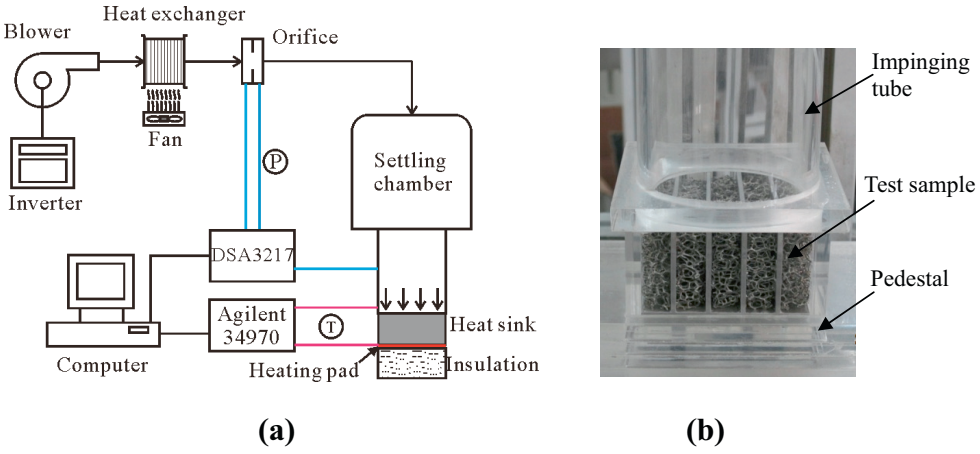

Fig. 3. Test rig details: (a) test setup of impingement experiment; (b) photo of test section.

2.3. Experimental data reduction

The jet Reynolds number is defined as:

$$\mathrm{Re} = \frac{\rho_f V_j D}{\mu_f} \tag{1}$$

where V_j is the jet exit velocity, which is the volume flow rate divided by the nozzle area. The jet velocity range tested was from 0.5 to 3 m/s, corresponding to the Reynolds number in the range of 3000 to 12,000.

The dimensionless pressure drop is defined as:

$$C_f = \frac{\Delta P}{0.5\rho_f V_j^2} \tag{2}$$

where ΔP is the pressure difference between the measured inet static pressure and the atmosphere pressure. Note that the air is discharged directly to the ambient after passing through the heat sink, thus the static pressure at the exit of heat sink is almost the same as the atmosphere pressure.

The overall heat transfer coefficient is calculated by:

$$h = \frac{Q}{A_b(T_w - T_{in})} = \frac{UI}{A_b(T_w - T_{in})} \tag{3}$$

where T_w is the facet average substrate temperature, and T_{in} is the inlet air temperature, i.e., the jet exit temperature.

The Nusselt number is then defined as:

$$Nu = \frac{hD}{k_f} \tag{4}$$

2.4. Uncertainty analysis

The uncertainties associated with the voltage and current measurements are 0.6% and 1%, respectively, while the uncertainty of the temperature measurements is estimated to be 2.5%. According to the method of Kline and McClintock [25], the uncertainty of the heat transfer coefficient defined in Eq. (3) can be calculated, as:

$$\frac{\delta h}{h} = \sqrt{\left(\frac{\delta U}{U}\right)^2 + \left(\frac{\delta I}{I}\right)^2 + \left(\frac{\delta T_w}{T_w - T_{in}}\right)^2 + \left(\frac{\delta T_{in}}{T_w - T_{in}}\right)^2} \tag{5}$$

Following the Eq. (5), the $\delta h/h$ here is estimated to be 3.8%. If the uncertainties associated with geometrical parameters and thermal properties are ignored, the uncertainty of the Nusselt number is then identical as that associated with the heat transfer coefficient. Similarly, the maximum uncertainties of the pressure drop and the Reynolds number are estimated to be 8.8% and 2.1% respectively, at Re = 8000.

3. Numerical model

3.1. Model assumptions

As shown in Fig. 4, the problem under consideration in numerical modeling is a FMF heat sink subjected to a circular impinging air jet. The circular nozzle is directly positioned on the top surface of the heat sink, and the region beyond the circular nozzle is confined by a thermal insulation wall. The two side surfaces are hydraulically impermeable and adiabatic. Due to the high thermal conductivity of aluminum, the temperature distribution on the substrate is in general uniform; and hence a constant temperature boundary condition ($T_w > T_{in}$) was specified at the substrate.

Due to the symmetrical nature of the thermal-fluid flow behavior in the heat sink, only one quarter of the heat sink was modeled as the computational domain, shown in Fig. 4. The computational domain includes only the plate-fins and the metal foams; and the thermal-fluid flow in the substrate and in the jet tube was not considered.

Other assumptions made in the numerical model include: (1) thermal contact resistance between the metal foam and the plate-fin is negligible; (2) metal foam is homogenous and isotropic; (3) fluid flow is steady state, laminar and incompressible; (4) thermo-physical properties of both the fluid and the foam are independent of temperature; (5) thermal dispersion in the metal foam is negligible since air is used as the coolant [9,10]; (6) buoyancy force and thermal radiation are neglected.

3.2. Governing equations and boundary conditions

Based on the above assumptions, the governing equations for conjugated heat transfer in plate-fins and metal foams are presented in this section. The origin of the coordinate system is located at the bottom center of the heat sink as shown in Fig. 4.

The fluid flow in the metal foam is described with the Darcy's extended equation as follows:

$$\nabla \cdot \langle \boldsymbol{u} \rangle = 0 \tag{6}$$

$$\frac{\rho_f}{\varepsilon}\nabla(\langle \boldsymbol{u} \rangle \langle \boldsymbol{u} \rangle) = -\varepsilon \nabla \langle p \rangle^f + \mu_f \nabla^2 \langle \boldsymbol{u} \rangle - \frac{\varepsilon \mu_f}{K}\langle \boldsymbol{u} \rangle - \frac{\varepsilon \rho_f c_E}{\sqrt{K}}|\langle \boldsymbol{u} \rangle|\langle \boldsymbol{u} \rangle \tag{7}$$

where the third term at the right hand side (RHS) of Eq. (7) is the well known Darcy's term, the second and the last terms are the non-Darcy terms proposed by Vafai and Tien [26] to account for

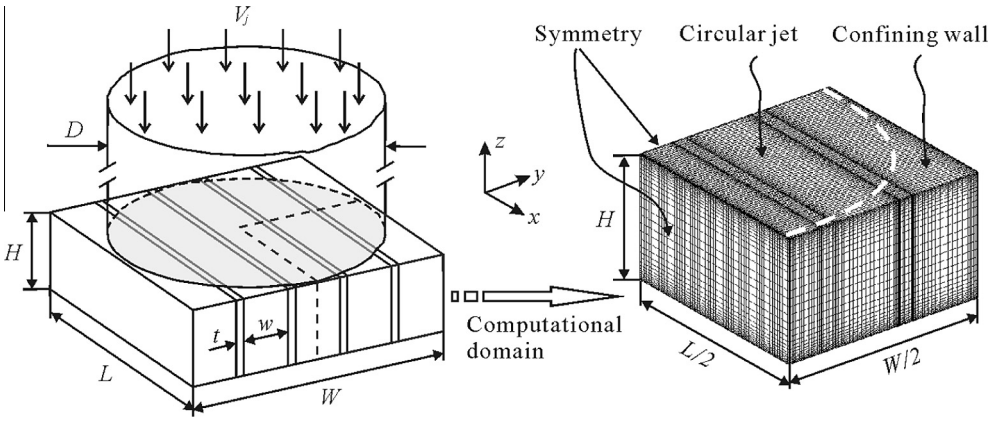

Fig. 4. Computational domain and grids.

the boundary and inertial effects, K is the permeability, c_E is the form drag coefficient, and ε is the porosity.

A local thermal non-equilibrium between the fluid and the solid within the metal foam is assumed. The heat transfer equations can be written as follows:

$$k_{se}\nabla^2\langle T_s\rangle^s - h_{sf}A_{sf}(\langle T_s\rangle^s - \langle T_f\rangle^f) = 0 \tag{8}$$

$$\rho_f c_{p,f}\nabla\cdot(\langle \boldsymbol{u}\rangle\langle T_f\rangle^f) = k_{fe}\nabla^2\langle T_f\rangle^f + h_{sf}A_{sf}(\langle T_s\rangle^s - \langle T_f\rangle^f) \tag{9}$$

where ρ_f, $c_{p,f}$ and μ_f are the density, the specific heat and the viscosity of air respectively; k_{fe} and k_{se} are the effective thermal conductivity of the fluid and the solid respectively; h_{sf} is the interstitial heat transfer coefficient between the fluid and the solid; and A_{sf} is the surface area density (wetted surface area per unit volume). The coupled heat transfer in plate-fins is governed by the steady-state heat conduction equation, as:

$$k_p\nabla^2 T_p = 0 \tag{10}$$

where k_p is the thermal conductivity of the plate-fin material.

It should be pointed out that, in Eqs. (6)–(10), $\langle\phi\rangle$ denotes the extrinsic average of a quantity over a volume containing both the fluid and the solid, and $\langle\phi\rangle^f$ and $\langle\phi\rangle^s$ refer to the intrinsic averages over a volume containing only the fluid and the solid, respectively. The extrinsic and intrinsic average of a generic transport variable is defined as [27]:

$$\langle\phi\rangle = \varepsilon\langle\phi\rangle^f, \quad \langle\phi\rangle = (1-\varepsilon)\langle\phi\rangle^s \tag{11}$$

For flow equations, non-slip boundary conditions were applied at wall surfaces. The convective heat dissipation at the inlet (including the fin tip and the foam region that are directly under jet impingement) was considered. At the exit, an adiabatic boundary condition was assumed for the solid-phase heat transfer equation as the temperature of air is heated up upon penetrating the heat sink. The temperature and heat flux continuity was assumed at the interfaces between the plate-fins and the foam. Mathematically, boundary conditions at different locations are given below.

At the heat sink inlet, i.e., $z = H, r < D/2$, for the foam region directly under jet impingement:

$$\begin{aligned}&\langle u\rangle = \langle v\rangle = 0, \quad \langle w\rangle = -V_{in},\\ &\langle T_f\rangle^f = T_{in}, -k_{se}\frac{\partial\langle T_s\rangle^s}{\partial z} = h_{foam}(\langle T_s\rangle^s - T_{in})\end{aligned} \tag{12}$$

for the fin tip directly under jet impingement:

$$\langle u\rangle = \langle v\rangle = \langle w\rangle = 0, \quad -k_p\frac{\partial T_p}{\partial z} = h_p(T_p - T_{in}) \tag{13}$$

At the top surface, for the region beyond the inlet, i.e., $z = H, r \geqslant D/2$:

$$\langle u\rangle = \langle v\rangle = \langle w\rangle = 0, \quad \frac{\partial T_p}{\partial z} = \frac{\partial\langle T_s\rangle^s}{\partial z} = \frac{\partial\langle T_f\rangle^f}{\partial z} = 0 \tag{14}$$

At the exit plane, i.e., $x = L/2$:

$$\frac{\partial\langle u\rangle}{\partial x} = \frac{\partial\langle v\rangle}{\partial x} = \frac{\partial\langle w\rangle}{\partial x} = 0, \quad \frac{\partial T_p}{\partial x} = \frac{\partial\langle T_s\rangle^s}{\partial x} = \frac{\partial\langle T_f\rangle^f}{\partial x} = 0 \tag{15}$$

At the symmetry plane of $x = 0$:

$$\frac{\partial\langle v\rangle}{\partial x} = \frac{\partial\langle w\rangle}{\partial x} = 0, \quad \langle u\rangle = 0, \quad \frac{\partial T_p}{\partial x} = \frac{\partial\langle T_s\rangle^s}{\partial x} = \frac{\partial\langle T_f\rangle^f}{\partial x} = 0 \tag{16}$$

At the symmetry plane of $y = 0$:

$$\frac{\partial\langle u\rangle}{\partial y} = \frac{\partial\langle w\rangle}{\partial y} = 0, \quad \langle v\rangle = 0, \quad \frac{\partial\langle T_s\rangle^s}{\partial y} = \frac{\partial\langle T_f\rangle^f}{\partial y} = 0 \tag{17}$$

At the side wall, i.e., $y = W/2$:

$$\langle u\rangle = \langle v\rangle = \langle w\rangle = 0, \quad \frac{\partial\langle T_s\rangle^s}{\partial y} = \frac{\partial\langle T_f\rangle^f}{\partial y} = 0 \tag{18}$$

At the bottom wall of $z = 0$:

$$\langle u\rangle = \langle v\rangle = \langle w\rangle = 0, \quad T_p = \langle T_s\rangle^s = \langle T_f\rangle^f = T_w \tag{19}$$

At the interface between the plate-fins and the foam:

$$\langle u\rangle = \langle v\rangle = \langle w\rangle = 0, \quad T_p = \langle T_s\rangle^s = \langle T_f\rangle^f, \quad -k_p\frac{\partial T_p}{\partial y} = -k_{se}\frac{\partial\langle T_s\rangle^s}{\partial y} - k_{fe}\frac{\partial\langle T_f\rangle^f}{\partial y} \tag{20}$$

Since high porosity open-cell metal foams are typically composed of inter-connected slender cylinders, in Eq. (12), the convective heat transfer coefficient between the foam and incoming flow may be determined using the correlation for staggered cylinders in crossflow [28]:

$$Nu_{foam} = \frac{h_{foam}d_f}{k_f} = \begin{cases} 0.76\mathrm{Re}_d^{0.4}\mathrm{Pr}^{0.37}, & (10^0 \leqslant \mathrm{Re}_d \leqslant 4\times10^1)\\ 0.52\mathrm{Re}_d^{0.5}\mathrm{Pr}^{0.37}, & (4\times10^1 \leqslant \mathrm{Re}_d \leqslant 10^3)\\ 0.26\mathrm{Re}_d^{0.6}\mathrm{Pr}^{0.37}, & (10^3 \leqslant \mathrm{Re}_d \leqslant 2\times10^5)\end{cases} \tag{21}$$

where Re_d is the Reynolds number based on the ligament diameter, as:

$$\mathrm{Re}_d = \rho_f V_{in} d_f/\mu_f \tag{22}$$

In Eq. (13), the convective heat transfer coefficient at the fin tip can be determined using the correlation of impinging flow on a flat plate [29,30]:

$$\begin{aligned}&h_p = k_f/t\cdot 0.6\cdot\mathrm{Re}_1^{0.5}\\ &\mathrm{Re}_1 = \rho_f\cdot V_j\cdot t/\mu_f\end{aligned} \tag{23}$$

3.3. Numerical procedure and data reduction

The governing equations were solved using the finite-volume method. A staggered grid system was employed, where the velocities were stored at the control-volume faces whilst all other variables were calculated at the grid points. The numerical method used is based on the SIMPLE algorithm. The discretized equations for each variable were solved by the line-by-line procedure which is a combination of the Tri-Diagonal-Matrix Algorithm (TDMA) and the Gauss–Seidel iteration technique of Patankar [31]. The iteration was terminated when changes in target variables were less than 10^{-6} between successive iterations. The grids were non-uniformly distributed with a large concentration of nodes near walls, as shown in Fig. 4. With the first node set at 0.1 mm away from the wall, the resulting grids of 60 (x) × 94 (y) × 40 (z) were found sufficient to obtain grid independent results. The Fortran code used in the computation has been validated for conjugated heat transfer problems [32,33].

To obtain the numerical heat transfer coefficient defined in Eq. (3), the total heat transfer rate of the heat sink needs to be known, including the heat transfer of the metal foam and that from the plate-fins:

$$Q = 4.\left\{\int_A\int_{foam}\left[-k_{se}\frac{\partial\langle T_s\rangle^s}{\partial}z\Big|_{z=0} - k_{fe}\frac{\partial\langle T_f\rangle^f}{\partial z}\Big|_{z=0}\right]dxdy + \int_A\int_{fin}\left[-k_p\frac{\partial T_p}{\partial z}\Big|_{z=0}\right]dxdy\right\} \tag{24}$$

where the multiplier "4" in Eq. (24) is due to the fact that the computational domain included only one quarter of the physical heat sink; A_{foam} and A_{fin} are the base area of the plate-fins and the foam in the computational domain, respectively.

The experimentally measured pressure drop includes two terms: (1) pressure drop of flow in the foam-filled fin channel; (2) pressure drop caused by contraction and expansion of flow at the inlet and the exit of the heat sink, i.e.,

$$\Delta P = \Delta P_{ch} + (\Delta P_i - \Delta P_e) \tag{25}$$

The inlet and exit pressure drop can be estimated using the empirical model for calculating the pressure drop due to flow entering and exiting a conventional plate-fin heat sink [34]. It was found that the inlet and exit pressure drop contributes less than 5% of the total pressure drop and can be ignored in current analysis. Therefore, the measured pressured drop is almost identical to ΔP_{ch}, which can be predicted from the model as:

$$\Delta P \approx \Delta P_{ch} = \frac{1}{A_i}\int\int_{A_i} p(x,y,H)dxdy - \frac{1}{A_e}\int\int_{A_e} p(L/2,y,z)dydz \tag{26}$$

where A_i is the inflow surface area and A_e is the outflow surface area.

4. Determination of foam properties

The thermal properties of aluminum foam (e.g., K, c_E, k_{se}, $h_{sf}A_{sf}$) need to be determined to solve Eqs. (6)–(10). The porosity of the foam was measured to be 0.963 by weighing the foam sample of volume 68 × 68 × 30 mm^3. The average fiber diameter was measured to be 0.47 mm using a caliper. The effective thermal conductivity of the foam is solely a function of porosity as demonstrated in several studies [35–37]. However, the flow associated thermal properties (K, c_E, $h_{sf}A_{sf}$) strongly depend on the cellular structure of the foam, such as fiber shape, fiber diameter, cell morphology, cell size, surface roughness, etc. These properties were experimentally determined under duct flow forced convection condition following the method given in Ref. [10].

Fig. 5(a) shows the setup of the duct flow forced convection experiment. The air flow after the settling chamber in Fig. 3(a) was led to a straight rectangular tube (cross-sectional area 68 × 30 mm^2) of length 970 mm. The metal foam heat sink of height 30 mm in Table 1 was placed in the rectangular tube 700 mm away from the leading-edge. A thin-wall metallic honeycomb was located upstream of the test sample to ensure a fully developed uniform flow. A constant heat flux was applied at the substrate by a heating pad. The pressure drop across the sample and substrate temperatures were measured for the inlet air velocity in a range of 0–5 m/s.

The permeability and inertial coefficients were obtained by data fitting using the measured pressure drop based on the Forchheimer extended Darcy's equation:

$$-\frac{dp}{dx} = \frac{\mu_f\langle u\rangle}{K} + \frac{\rho_f c_E}{\sqrt{K}}\langle u\rangle^2 \tag{27}$$

and results are K = 3.142 × 10^{-7} m^2 and c_E = 0.0492, respectively.

The volumetric heat transfer coefficient h_v (=$h_{sf}A_{sf}$) was determined by data fitting using the measured temperature based on the porous medium model. The porous medium model for duct flow is shown in Fig. 5(b) as a conjugated heat transfer between aluminum foam and substrate. Due to symmetry, only half of the foam heat sink was considered. The governing equations for the fluid flow and the heat transfer in the foam are the same as Eqs. (6)–(9), while the heat transfer in the substrate is governed by Eq. (10). A constant heat flux q'' was applied at the substrate surface, and uniform velocity and temperature were assumed at the inlet. Detailed boundary conditions for the duct flow configuration are:

$$\langle u\rangle = u_0, \langle T_f\rangle^f = T_{in}, \quad \frac{\partial\langle T_s\rangle^s}{\partial x} = \frac{\partial T_p}{\partial x} = 0 \quad \text{at left boundary} \tag{28}$$

$$\frac{\partial\langle u\rangle}{\partial x} = \frac{\partial\langle v\rangle}{\partial x} = \frac{\partial\langle w\rangle}{\partial x} = 0, \quad \frac{\partial T_p}{\partial x} = \frac{\partial\langle T_s\rangle^s}{\partial x} = \frac{\partial\langle T_f\rangle^f}{\partial x} = 0 \quad \text{at right boundary} \tag{29}$$

$$\frac{\partial\langle u\rangle}{\partial y} = \frac{\partial\langle w\rangle}{\partial y} = 0, \quad \langle v\rangle = 0, \frac{\partial\langle T_s\rangle^s}{\partial y} = \frac{\partial\langle T_f\rangle^f}{\partial y} = \frac{\partial T_p}{\partial y} = 0 \quad \text{at front boundary} \tag{30}$$

$$\langle u\rangle = \langle v\rangle = \langle w\rangle = 0, \quad \frac{\partial\langle T_s\rangle^s}{\partial y} = \frac{\partial\langle T_f\rangle^f}{\partial y} = \frac{\partial T_p}{\partial y} = 0 \quad \text{at back boundary} \tag{31}$$

$$\langle u\rangle = \langle v\rangle = \langle w\rangle = 0, \quad k_s\frac{\partial T_p}{\partial z} = q'' \quad \text{at top boundary} \tag{32}$$

$$\langle u\rangle = \langle v\rangle = \langle w\rangle = 0, \quad \frac{\partial\langle T_s\rangle^s}{\partial z} = \frac{\partial\langle T_f\rangle^f}{\partial z} = 0 \quad \text{at bottom boundary} \tag{33}$$

When solving Eqs. (6)–(10) with the above boundary conditions, the volumetric heat transfer coefficient h_v(=$h_{sf}A_{sf}$) was adjusted to ensure that the predicted heat transfer coefficient was within 0.5% of the experimental data at each inlet velocity. The resulting h_v of the aluminum foam is correlated as a function of the inlet velocity (or Darcy velocity), as:

$$h_v = h_{sf}A_{sf} = 8350 \cdot u_0^{0.45} \tag{34}$$

For comparison, for commercially available ERG aluminum foams, the relation between interstitial heat transfer coefficient and velocity is correlated as $h_{sf} \sim u_0^{0.5}$ [10]. The small difference in the exponent of the velocity may be attributed to the different microstructures of the present foam and the ERG foam.

The thermal properties of the aluminum foam are summarized in Table 2 (note that when Eq. (34) is applied for the impinging flow condition, the local Darcy velocity should be used instead of u_0). Since the boundary layer thickness is very thin for the flow in the foam, the velocity distribution in the foam filled duct is almost uniform. Meanwhile, the thermal properties of a given foam vary only with the local flow velocity. Once the thermal properties of the given foam are determined under the duct flow condition (approximately a uniform velocity condition), then they can be

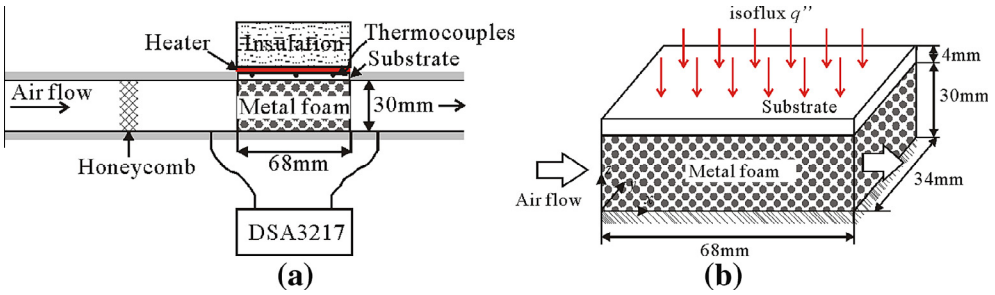

Fig. 5. Determination of foam properties: (a) duct flow experiment; (b) duct flow numerical model.

Table 2
Thermal properties of aluminum foam.

PPI/–	ε/(–)	d_f/m	K/m^2	c_E	k_{se}/(W/m K)[a]	k_{fe}/(W/m K)[a]	h_v/(W/m^3 K)
8	0.963	0.00047	3.142×10^{-7}	0.0492	2.6	0.0246	$8350 \cdot \left(\sqrt{\langle u\rangle^2 + \langle v\rangle^2 + \langle w\rangle^2}\right)^{0.45}$

[a] Calculated from the model in Ref. [35].

employed for FMF and MF heat sinks under more complicated flow conditions such as impinging flow.

5. Results and discussion

5.1. Verification of the model

In order to verify the numerical model and the numerical procedure presented in Section 3, the computational cases in Ref. [27] have been repeated using our own code. In Ref. [27], the thermal performance of MF and FMF heat sinks under duct flow forced convection were numerically investigated, where the foam sample has a porosity of 0.9005, mean pore and ligament diameters of 2.58 and 0.35 mm, respectively; and different numbers of fins, i.e. 1, 2, 4, 6 and 8 were considered. In the current calculation, the same foam properties and fin dimensions were used as those given in Ref. [27]. Fig. 6 compares the simulation results obtained using our own code with those in [27] for MF and 4-fin FMF cases, which shows good agreements. The discrepancy for 4-fin FMF case in the high velocity region may be caused by the different values used in the current study for the thermal conductivity of the fin as well as air properties, since these were not detailed in Ref. [27].

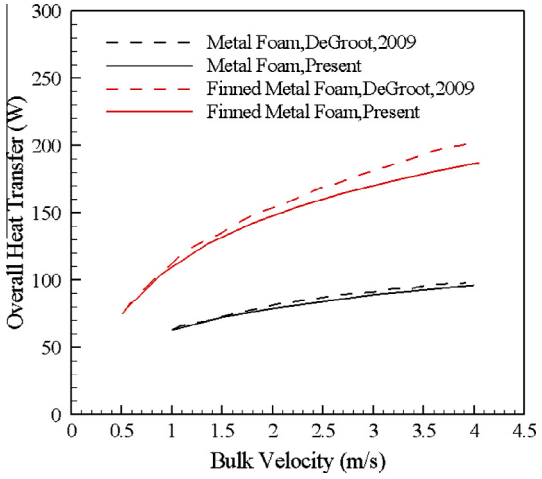

Fig. 6. Comparison of the overall heat transfer between the current calculation and Ref. [27] for MF and 4-fin FMF cases under the duct flow condition, $T_w - T_{in} = 50$ K.

5.2. Local fluid-flow and temperature distributions characteristics

Fig. 7 shows streamlines in (a) MF and (b) FMF heat sinks, both with a height of 20 mm, revealing the basic flow characteristics. Due to symmetry, only one quarter of each heat sink is shown. Flows in both the MF and FMF heat sinks are basically in accordance with impinging jet behavior: the flow turns 90° after stagnation at the impinging plate and then stays parallel to the plate. However, different flow behaviors are observed in the MF and FMF heat sinks under circular impinging jet. The flow in the MF heat sink, as shown in Fig. 7 (a), not only turns 90° in the x–z plane, but also change direction in the x–y plane, which ends up approaching the side wall of the heat sink. This is attributed to the non-uniform injection of the air flow rate along the y direction. For the FMF heat sink, due to the existence of the plate-fins, the y-velocity component is restricted; therefore the flow in each slice of y can be regarded as a two-dimensional impinging jet.

In order to further illustrate this behavior, the velocity vectors in the mid-z plane of both the MF and FMF heat sinks are shown in Fig. 8(a) and (b), respectively. Fig. 8(a) shows a uniform velocity profile at the exit of the MF heat sink, suggesting that the porous foam has very good performance in terms of evening the flow. Contrary to the MF heat sink, a non-uniform flow distribution is clearly observed at the exit of the FMF heat sink due to restriction of the flow by the plate-fins.

Fig. 9 shows fluid- and solid- temperature distributions in MF and FMF heat sinks, both with a typical height of 20 mm. For either heat sink, temperature differences between two-phases (fluid and solid) can be clearly observed, implying that the local thermal non-equilibrium prevails in the foam/air system, therefore, the two-equation model is required to account for the heat transfer of each phase. For the solid-temperature distribution of the MF heat sink shown in Fig. 9(b), it was found that the temperature of the foam decreases rapidly along the foam height. In the region above the middle height, the temperature of the foam is only slightly higher than the fluid-temperature, which makes the heat transfer in this region much less efficient. As a result, increasing the foam height will not lead to better heat transfer, or even worse, may inversely decrease the heat transfer (see Fig. 10(a)), despite that the total available heat transfer area is increased. This is caused by the fact that the increased heat transfer area is very inefficient, and meanwhile, the amount of air reaching the base is reduced as the foam height is increased

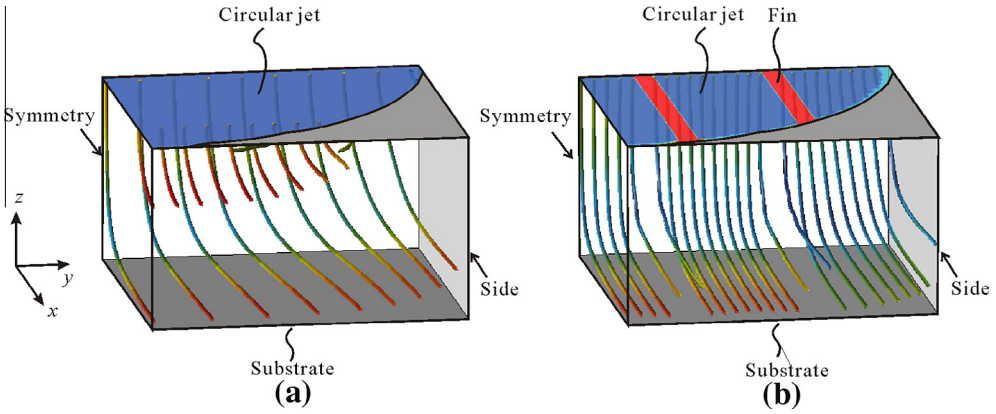

Fig. 7. Illustration of streamlines at a height of 20 mm: (a) MF and (b) FMF.

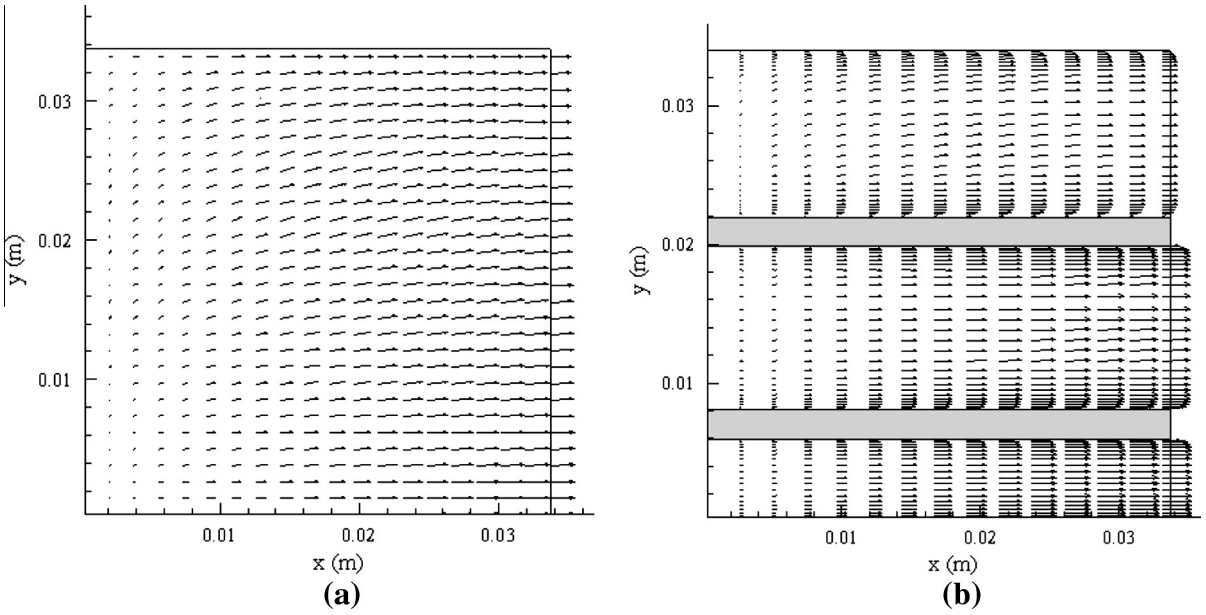

Fig. 8. Velocity vectors in mid-*z* plane at a height of 20 mm: (a) MF and (b) FMF.

[17]. For the FMF heat sink, as the plate-fins promote heat conduction from the substrate into foam blocks, the foam temperature (see Fig. 9(d)) is significantly higher than that in the MF heat sink. Therefore, the heat transfer of the FMF heat sink is greatly enhanced as a result of the larger temperature difference between the fluid and the solid.

5.3. Comparison to experiments and key influencing factors of the model predictions

Fig. 10 compares the heat transfer results between experimental measurements and numerical calculations for (a) MF and (b) FMF heat sinks. For both heat sink types, the Nusselt number increases with increasing Reynolds number. The numerical model predicted the overall trend correctly. For MF heat sinks with $H = 30$ mm, the agreement between experiment and modeling is well within the estimated uncertainty of Nusselt number; for those with $H = 20$ mm and $H = 10$ mm, the model over-predicts the Nusselt number by 9% and 11%, respectively. For FMF heat sinks with $H = 10$ mm and $H = 20$ mm, the numerical and experimental results agree well; whilst for $H = 30$ mm, the model under-predicts the Nusselt number by 13%. Given the complex structure of the foam and the impinging system, it appears that the accuracy of the model adopting the laminar Darcy's extended flow equations may be acceptable from an engineering point of view.

Within the range of the foam height (10–30 mm) considered, the heat transfer of the MF heat sink decreases monotonically as the foam height increases. However, the heat transfer of the FMF heat sink first increases as the foam height increases from $H = 10$ to 30 mm, then slightly decreases when H further increases to 40 mm. Fig. 11 shows that the model predicts correctly the dependency of heat transfer on foam height (H) for both heat sink types. Shih et al. [17] experimentally investigated two conflicting effects of foam height on the heat transfer of aluminum-foam cylinder under circular impinging air jet. They tested a foam sample of 20 PPI and 0.87 porosity, and found that the Nusselt number first increases and then decreases when the foam height decreases from 60 to 10 mm (the optimal height is ~15 mm). They explained that the increase in the Nusselt number with decreasing foam height is caused by the increasing percentage of cooling air reaching the heated surface, due to reduced flow resistance. The decrease in the Nusselt number with decreasing foam height is mainly caused by the reduction in the heat transfer area between the cooling air and the foam. It can be further inferred that if the heat conduction capability of a foam block is stronger, the optimal foam height is higher. This is because for a foam block with good heat conduction

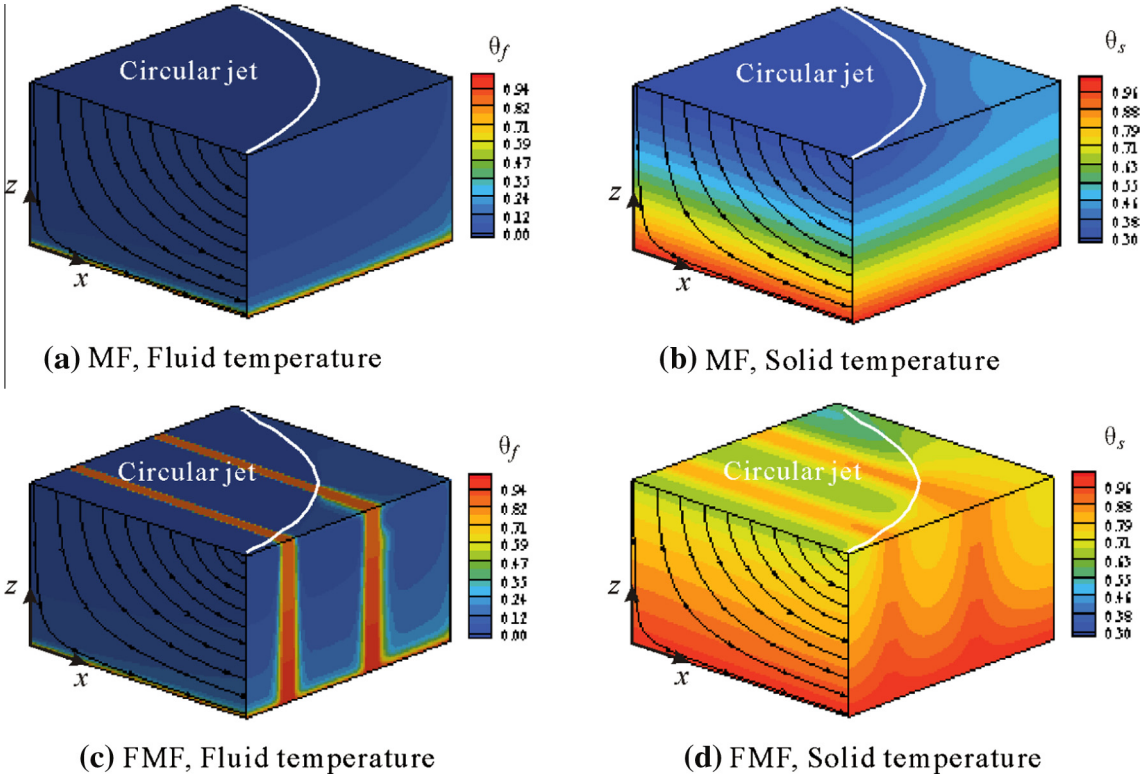

Fig. 9. Temperature distribution: (a) MF, fluid-temperature; (b) MF, solid-temperature; (c) FMF, fluid-temperature; (d) FMF, solid-temperature. Streamlines on the $y = 0$ surface are also included.

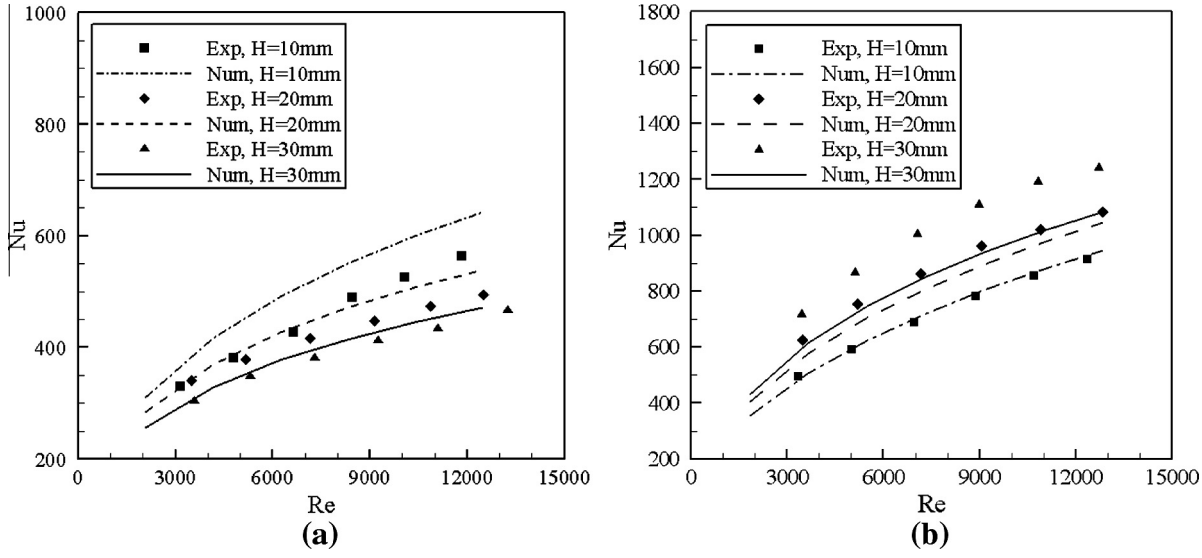

Fig. 10. Nusselt numbers plotted as a function of Reynolds number for (a) MF and (b) FMF heat sinks having different heights.

capability, the increasing heat transfer area with increasing foam height is more efficient. Therefore, the optimal height (30–40 mm) of the current tested FMF heat sinks is higher than that (~15 mm) of the regular foam sample in Shih et al. [17]. On the other hand, the current foam samples have a higher porosity of 0.963, and their effective thermal conductivity is smaller than that of the foam sample tested by Shih et al. [17], whose porosity was 0.87; therefore, the optimal height was not observed in the current study within the range of the height tested.

Fig. 12 compares the pressure drop obtained from experiments and modeling as a function of jet velocity for (a) MF and (b) FMF heat sinks. For both heat sink types, the model predicts the variation of pressure drop with jet exit velocity and foam height correctly. The pressure drop shows as a quadratic function of the jet velocity, indicating that the flow is in the non-Darcy regime where the inertial effect dominates. The pressure drop increases dramatically with decreasing foam height at the same jet velocity (or same volumetric flow rate). This is mainly caused by the higher flow velocity in the foam with a lower height due to smaller flow area.

With good agreements achieved between model predictions and experimental measurements in terms of both heat transfer and pressure drop, the numerical model is used next to assess

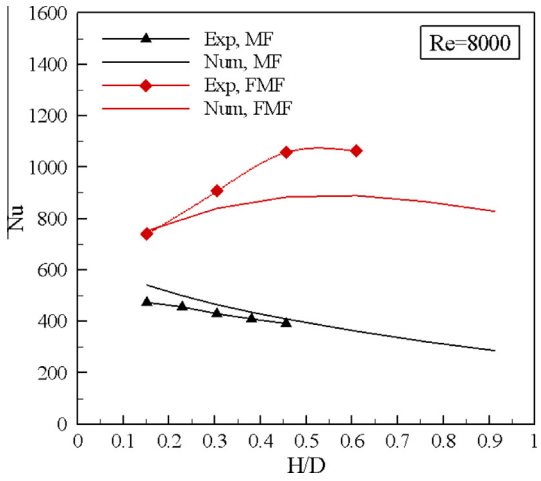

Fig. 11. Effect of foam height on heat transfer for both MF and FMF heat sinks.

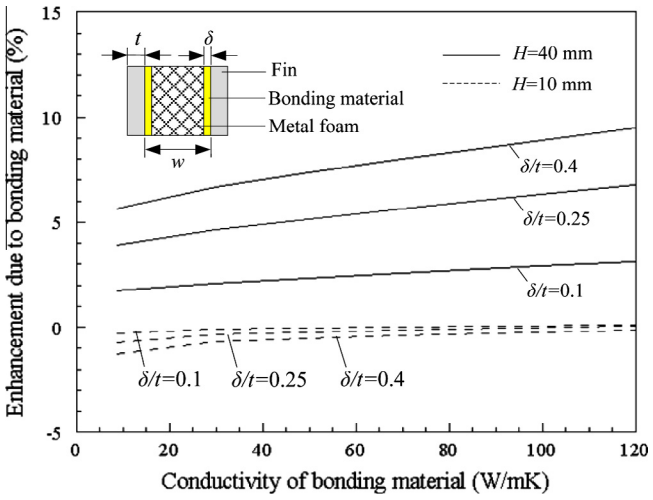

Fig. 13. Influence of the bonding material on heat transfer of FMF at Re = 11,000.

the influence of several key factors on the heat transfer of FMF heat sinks, including the bonding material and the inlet thermal boundary condition.

As shown in Fig. 11, for FMF heat sinks, the Nusselt number measured by the experiment is higher than that predicted by the numerical model at large foam heights. Zhao and Lu et al. [38] and DeGroot et al. [27] obtained similar results, and they argued that this could be attributed to the bonding material, which was not considered in the modeling. However, no quantitative assessment was given on the influence of the bonding material. In this study, a thin layer of bonding material of thickness δ between the plate-fins and the foam was considered in the numerical model, as schematically shown in Fig. 13. The bonding material occupied one grid point in the y direction, and the thermal conductivity of the bonding material was specified differently from that of the fin material. Fig. 13 shows the influence of the bonding materials of different thicknesses and thermal conductivities with two typical fin heights of $H = 10$ and 40 mm. For FMF heat sinks at a relatively large height, e.g. $H = 40$ mm, the Nusselt number considering the bonding material is 2–9% higher than that without considering it. This is mainly because that the bonding material increases the effective thickness of the fins which promotes heat conduction from the substrate into the foam; and also partially due to increased air velocity with reduced flow area. For the FMF samples in this study, the bonding material has a thickness of 0.2–0.3 mm and a thermal conductivity of 8.8 W/m K, and at $H = 40$ mm the enhancement caused by the bonding material is ~2%. At a smaller height, e.g. $H = 10$ mm, a slight reduction in the heat transfer was observed with the bonding material. This is because that the bonding material adds a small thermal resistance between the plate-fins and the foam.

When modeling heat transfer of a porous heat sink under impinging jet cooling, the exact thermal boundary condition at the inlet is unknown. Literature studies adopted either an adiabatic condition [39] or a constant temperature [40] for the solid-phase energy equation. The real thermal boundary condition should be between these two limiting cases. For a metal foam block under slot jet impingement, Jeng and Tzeng [12] compared the results obtained by using the adiabatic boundary condition and that by using the constant temperature boundary condition. Hwang et al. [41] showed that the inlet thermal boundary condition has significant influence on local heat transfer distribution in sintered bronze beads filled duct.

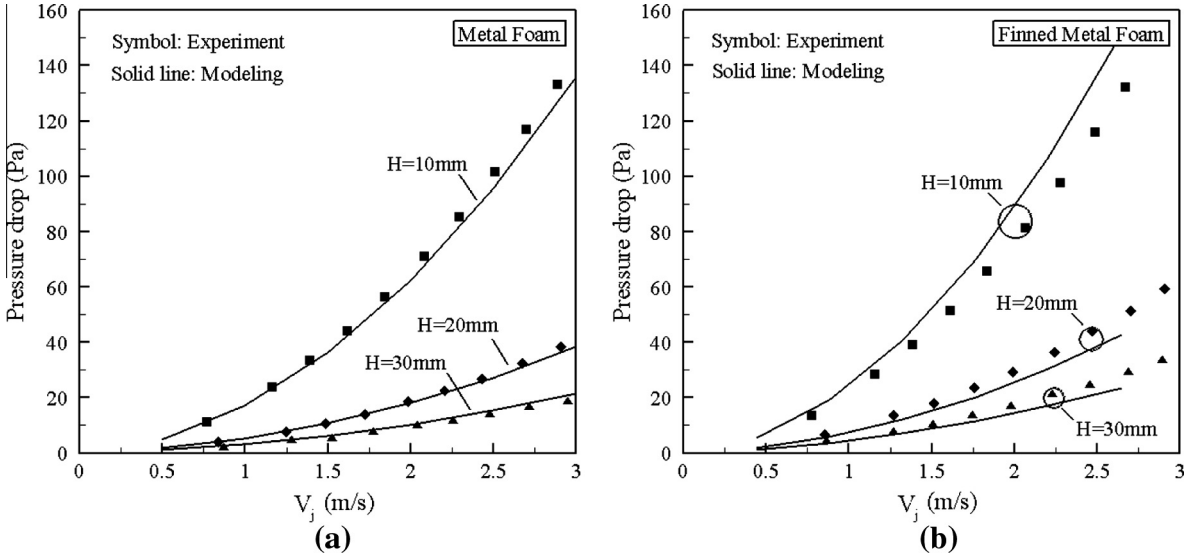

Fig. 12. Pressure drop plotted as a function of jet velocity for (a) MF and (b) FMF heat sinks.

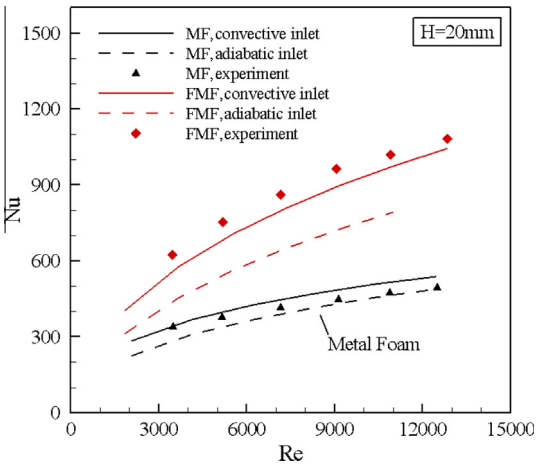

Fig. 14. Effect of inlet thermal boundary condition on numerical predictions.

In this study, a convective thermal boundary condition at the inlet was used for FMF heat sinks under impinging jet cooling, as given in Eqs. (21)–(23). Fig. 14 compares the Nusselt number predicted using the convective thermal boundary condition with that using the adiabatic condition for both MF and FMF heat sinks with $H = 20$ mm; and experimental data are also included for benchmarking. It is shown that for MF heat sinks, the influence of the inlet thermal boundary condition is relatively small. This is because that the temperature difference between the foam tip and the incoming air is small (see Fig. 9); and consequently, the convective heat dissipation at the inlet is negligible. However, for FMF heat sinks, the convective heat dissipation at the inlet is not negligible, and the adiabatic boundary condition leads to significant under-predictions of the heat transfer comparing with the experimental data.

5.4. Comparison of the thermal performance between FMF and MF

The thermal performance of FMF heat sinks was compared with that of MF heat sinks under both a fixed flow rate and a fixed pumping power conditions. Fig. 15(a) plots the ratio of the Nusselt number of the FMF heat sink to that of the MF heat sink with the same overall height as a function of the Reynolds number. It is shown that, at a given Reynolds number (or given volumetric flow rate), the heat transfer of the FMF heat sink is 1.5–2.8 times of that of the MF heat sink having the same overall height; and the enhancement increases as the height or the Reynolds number is increased.

In engineering applications such as electronics cooling, heat sinks are usually subjected to an axial fan impinging flow, where the flow rate is not fixed with different heat sinks due to the different pressure drop characteristics of the heat sinks. To compare thermal performance between FMF and MF heat sinks by considering the pressure drop penalty, Fig. 15(b) plots the Nusselt number as a function of the dimensionless pumping power (i.e., $C_f Re^3$) for both heat sinks with three different heights. It is found that at a given pumping power, for the MF heat sinks, the heat transfer is insensitive to the foam height; whilst for the FMF heat sinks, the heat transfer increases as the height increases. These findings are consistent with those observed for MF and FMF heat sinks under a typical axial fan impinging flow. Further, at a dimensionless pumping power of 6000, the heat transfer of the FMF heat sink is 1.5, 2, and 2.5 times that of the MF heat sink with $H = 10$, 20, and 30 mm, respectively.

6. Conclusions

A combined experimental and numerical study has been carried out on finned metal foam and metal foam heat sinks under impinging air jet cooling. Main conclusions are:

1. Under a given flow rate, for MF heat sinks, the heat transfer decreases monotonously as the foam height increases; whilst for FMF heat sinks, the heat transfer first increases and then slightly decreases as the foam height increases.
2. Under a given pumping power condition, for MF heat sinks, the heat transfer is insensitive to the foam height; whilst for FMF heat sinks, the heat transfer increases as the foam height increases.
3. Under either a given flow rate or a given pumping power condition, the heat transfer of FMF heat sinks could be 1.5–2.8 times that of MF heat sinks with the same foam height. The benefit of using FMF heat sinks instead of regular MF heat sinks is more pronounced at a larger foam height.

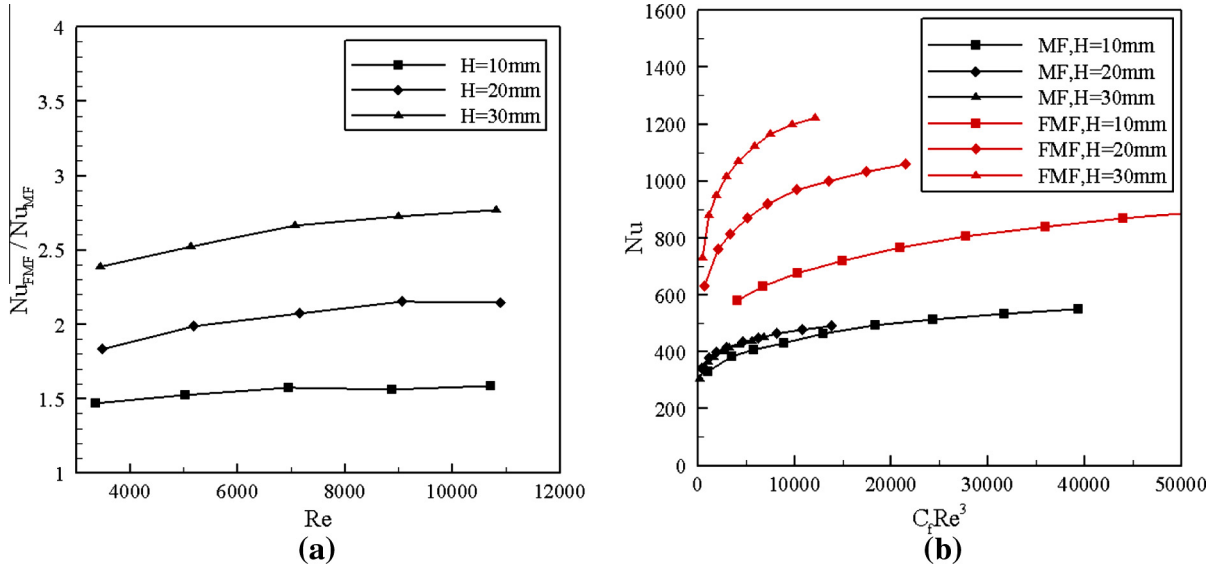

Fig. 15. Comparison of thermal performance between MF and FMF heat sinks at: (a) fixed flow rate; (b) fixed pumping power.

4. The bonding material enhances the heat transfer of FMF heat sinks at a large height (e.g., $H = 40$ mm). This is because the bonding material increases the effective thickness of the plate-fins and promotes the heat conduction into the foam blocks. However, since the bonding material adds a small thermal resistance between the plate-fins and the foam, at a small height (e.g., $H = 10$ mm), the heat transfer considering the bonding material is slightly lower than that without considering it.
5. When modeling the heat transfer of FMF heat sinks under impinging cooling, convective heat dissipation at the inlet should not be ignored.

Conflict of interest

None declared.

Acknowledgments

This work was supported by the National Natural Science Foundation of China (51206128), the National Basic Research Program of China (2011CB610305), the National "111" Project of China (B06024), China Postdoctoral Science Foundation funded project (2012M521766), Shaanxi Province Science Foundation funded project and the Fundamental Research Funds for the Central Universities of China. The authors also thank Mr. J. Wang for preparing the test samples.

References

[1] D.H. Lee, J. Song, M.C. Jo, The effects of nozzle diameter on impinging jet heat transfer and fluid flow, J. Heat Transfer – Trans. ASME 126 (4) (2004) 554–557.
[2] J.W. Baughn, S. Shimizu, Heat transfer measurements from a surface with uniform heat flux and an impinging jet, J. Heat Transfer – Trans. ASME 111 (1–4) (1989) 1096–1098.
[3] R.J. Goldstein, M.E. Franchett, Heat-transfer from a flat surface to an oblique impinging jet, J. Heat Transfer – Trans. ASME 110 (1) (1988) 84–90.
[4] H.Q. Yang et al., Flow structure, wall pressure and heat transfer characteristics of impinging annular jet with/without steady swirling, Int. J. Heat Mass Transfer 53 (19–20) (2010) 4092–4100.
[5] R. Viskanta, Heat transfer to impinging isothermal gas and flame jets, Exp. Therm. Fluid Sci. 6 (2) (1993) 111–134.
[6] K. Jambunathan et al., A review of heat transfer data for single circular jet impingement, Int. J. Heat Fluid Flow 13 (2) (1992) 106–115.
[7] C.Y. Zhao, Review on thermal transport in high porosity cellular metal foams with open cells, Int. J. Heat Mass Transfer 55 (13–14) (2012) 3618–3632.
[8] S.M. Kuo, C.L. Tien, Heat transfer augmentation in a foam-material filled duct with discrete heat sources, in: InterSociety Conference on Thermal Phenomena in the Fabrication and Operation of Electronic Components: I-THERM '88, 1988.
[9] M.L. Hunt, C.L. Tien, Effects of thermal dispersion on forced-convection in fibrous media, Int. J. Heat Mass Transfer 31 (2) (1988) 301–309.
[10] V.V. Calmidi, R.L. Mahajan, Forced convection in high porosity metal foams, J. Heat Transfer – Trans. ASME 122 (3) (2000) 557–565.
[11] T.J. Lu, H.A. Stone, M.F. Ashby, Heat transfer in open-cell metal foams, Acta Mater. 46 (10) (1998) 3619–3635.
[12] T.M. Jeng, S.C. Tzeng, Numerical study of confined slot jet impinging on porous metallic foam heat sink, Int. J. Heat Mass Transfer 48 (23–24) (2005) 4685–4694.
[13] T.-M. Jeng, S.-C. Tzeng, Forced convection of metallic foam heat sink under laminar slot jet confined by parallel wall, Heat Transfer Eng. 28 (5) (2007) 484–495.
[14] T.-M. Jeng, S.-C. Tzeng, Experimental study of forced convection in metallic porous block subject to a confined slot jet, Int. J. Therm. Sci. 46 (12) (2007) 1242–1250.
[15] A. Ejlali et al., Application of high porosity metal foams as air-cooled heat exchangers to high heat load removal systems, Int. Commun. Heat Mass Transfer 36 (7) (2009) 674–679.
[16] A. Marafie et al., Non-Darcian effects on the mixed convection heat transfer in a metallic porous block with a confined slot jet, Numer. Heat Transfer Part A – Appl. 54 (7) (2008) 665–685.
[17] W.H. Shih, W.C. Chiu, W.H. Hsieh, Height effect on heat-transfer characteristics of aluminum-foam heat sinks, J. Heat Transfer – Trans. ASME 128 (6) (2006) 530–537.
[18] S.Y. Kim, M.H. Lee, K.S. Lee, Heat removal by aluminum-foam heat sinks in a multi-air jet impingement, IEEE Trans. Compon. Packag. Technol. 28 (1) (2005) 142–148.
[19] J.J. Kuang et al., Ultralightweight compact heat sinks with metal foams under axial fan flow impingement, Heat Transfer Eng. 33 (7) (2012) 642–650.
[20] B.V. Antohe, J.L. Lage, A general two-equation macroscopic turbulence model for incompressible flow in porous media, Int. J. Heat Mass Transfer 40 (13) (1997) 3013–3024.
[21] H.M. Hofmann et al., Calculations of steady and pulsating impinging jets – an assessment of 13 widely used turbulence models, Numer. Heat Transfer Part B – Fundam. 51 (6) (2007) 565–583.
[22] A. Bhattacharya, R.L. Mahajan, Finned metal foam heat sinks for electronics cooling in forced convection, J. Electron. Packag. 124 (3) (2002) 155–163.
[23] A. Bhattacharya, R.L. Mahajan, Metal foam and finned metal foam heat sinks for electronics cooling in buoyancy-induced convection, J. Electron. Packag. 128 (3) (2006) 259–266.
[24] S. Krishnan et al., Design of complex structured monolithic heat sinks for enhanced air cooling, IEEE Trans. Compon. Packag. Manuf. Technol. 2 (2) (2012) 266–277.
[25] S.J. Kline, F.A. McClintock, Describing uncertainties in single-sample experiments, Mech. Eng. (1953) 3–8.
[26] K. Vafai, C.L. Tien, Boundary and inertia effects on flow and heat-transfer in porous-media, Int. J. Heat Mass Transfer 24 (2) (1981) 195–203.
[27] C.T. DeGroot, A.G. Straatman, L.J. Betchen, Modeling forced convection in finned metal foam heat sinks, J. Electron. Packag. 131 (2) (2009).
[28] A.A. Zukauskas, Convective heat transfer in cross-flow, in: S. Kakac, R.K. Shah, W. Aung (Eds.), Handbook of Single-Phase Convective Heat Transfer, Wiley, New York, 1987.
[29] Y. Kondo et al., Optimization of finned heat sinks for impingement cooling of electronic packages, J. Electron. Packag. 120 (3) (1998) 259–266.
[30] E.R.G. Eckert, R.M. Drake, Analysis of Heat and Mass Transfer, McGraw-Hill, NY, 1972, pp. 306–314.
[31] S.V. Patankar, Numerical Heat Transfer and Fluid Flow, McGraw-Hill, NY, 1980.
[32] S.S. Feng, T. Kim, T.J. Lu, Numerical investigation of forced convection in pin/plate-fin heat sinks heated by impinging jet using porous medium approach, Int. J. Numer. Methods Heat Fluid Flow 23 (1) (2013) 88–107.
[33] S.S. Feng, T. Kim, T.J. Lu, A semi-empirical heat transfer model for forced convection in pin-fin heat sinks subjected to nonuniform heating, J. Heat Transfer – Trans. ASME 132 (12) (2010).
[34] J. Tzer-Ming, T. Sheng-Chung, A semi-empirical model for estimating permeability and inertial coefficient of pin-fin heat sinks, Int. J. Heat Mass Transfer 48 (15) (2005) 3140–3150.
[35] A. Bhattacharya, V.V. Calmidi, R.L. Mahajan, Thermophysical properties of high porosity metal foams, Int. J. Heat Mass Transfer 45 (5) (2002) 1017–1031.
[36] Y.H. Yang, T.J. Lu, T. Kim, A simplistic model for the tortuosity in two-phase close-celled porous media, J. Phys. D – Appl. Phys. 46 (12) (2013).
[37] K. Boomsma, D. Poulikakos, On the effective thermal conductivity of a three-dimensionally structured fluid-saturated metal foam, Int. J. Heat Mass Transfer 44 (4) (2001) 827–836.
[38] C.Y. Zhao et al., Thermal transport in high porosity cellular metal foams, J. Thermophys. Heat Transfer 18 (3) (2004) 309–317.
[39] K. Dong-Kwon, K. Sung Jin, B. Jin-Kwon, Comparison of thermal performances of plate-fin and pin-fin heat sinks subject to an impinging flow, Int. J. Heat Mass Transfer 52 (15–16) (2009) 3510–3517.
[40] W. Kok-Cheong, N.H. Saeid, Numerical study of mixed convection on jet impingement cooling in a horizontal porous layer under local thermal non-equilibrium conditions, Int. J. Therm. Sci. 48 (5) (2009) 860–870.
[41] G.J. Hwang, C.C. Wu, C.H. Chao, Investigation of non-Darcian forced-convection in an asymmetrically heated sintered porous channel, J. Heat Transfer – Trans. ASME 117 (3) (1995) 725–732.